doi: 10.18720/MCE.78.11

Deformation compatibility of masonry and composite materials

Деформационная совместимость каменной кладки с композитными материалами

V.V. Bespalov,
Peter the Great St. Petersburg Polytechnic University, St. Petersburg, Russia
D. Ucer,
Middle East Technical University, Ankara, Turkey
I.D. Salmanov,
I.N. Kurbanov,
Peter the Great St. Petersburg Polytechnic University, St. Petersburg, Russia
S.V. Kupavykh,
Saint-Petersburg Mining University, St. Petersburg, Russia

Студент В.В. Беспалов,
Санкт-Петербургский политехнический университет Петра Великого, г. Санкт-Петербург, Россия
M.Sc., научный сотрудник Д. Ючер,
Middle East Technical University, Анкара, Турция
студент И.Д. Сальманов,
студент И.Н. Курбанов,
Санкт-Петербургский политехнический университет Петра Великого, г. Санкт-Петербург, Россия
канд. техн. наук, ведущий инженер С.В. Купавых
Санкт-Петербургский горный университет, г. Санкт-Петербург, Россия

Key words: masonry; FRP; simulation; deformation compatibility; composite materials; compression-bending element

Ключевые слова: каменная кладка; симуляция, поверхностное армирование; композитные материалы; сжато-изогнутые элементы; деформационная совместимость

Abstract. Fiber Reinforced Polymers (FRP) are commonly used nowadays for strengthening deteriorated structures. The purpose of this research was to determine the combined behavior of masonry walls and reinforcing meshes together, according to their deformation characteristics. A sample wall with average masonry parameters and seven different common polymer nets on them were modeled in Abaqus Software. Moreover, a case study wall was also modeled according to the strength values obtained from direct testing of a demolished masonry wall that was shaped as secondary blocks for reusing purposes. In addition to the analysis of this plain recovered wall, the strengthened version of it with carbon fiber polymer mesh was also modeled. The results obtained from the theoretical sample wall and the case study wall with plain and reinforced alternatives stated that; the compatibility of deformation characteristics between the wall and the reinforcing mesh is the key for combined strength behavior of the wall. Lastly, besides illustrating and discussing all the stress-strain conditions for the analyzed cases, this study also offered a formula for the detection of combined behavior in question, according to the material properties of unreinforced wall and reinforcing mesh separately. This formula is quite useful in order to decide to the suitable mesh type prior to the application.

Аннотация. Композитное поверхностное армирование обычно используются в настоящее время для усиления повреждённых конструкций. Цель исследования предполагала определение поведения кладки стен и армирующих сеток при их совместной работе с учётом их деформационных характеристик. Образец стены с усреднёнными характеристиками кладки и семь разновидностей композитного армирования были смоделированы в программном комплексе Abaqus. Кроме того, для оценки возможности применения подобной симуляции к реальным конструкциям, был произведён расчёт восстановленной каменной стены с учётом характеристик, полученных по результатам лабораторных испытаний. Учитывались случаи неармированной стены и стены с композитным поверхностным армированием. Результаты, полученные при моделировании условно принятой стены и практического случая, показали, что совместимость деформационных характеристик каменной стены и материала поверхностного армирования

Беспалов В.В., Ючер Д., Салманов И.Д., Курбанов И.Н., Купавых С.В. Деформационная совместимость каменной кладки с композитными материалами // Инженерно-строительный журнал. 2018. № 2(78). С. 136–150.

является ключевой в совместной работе всей конструкции. Также была предложена формула для определения степени деформационной совместимости в зависимости от свойств материала неармированной стены и поверхностного армирования. Определение деформационной совместимости может быть применимо при подборе вида поверхностного армирования.

1. Introduction

Unreinforced masonry has been widely used as a construction technique in the building industry throughout history. Most of these buildings are still in service and some of them require strengthening in order to adapt the structure to a new use or to fulfill the requirements of current regulations. Among the masonry structures, the most difficult ones to analyze are vaults and others under the impacts of compression and bending. Several prerequisites were proposed for calculating and evaluating the strength of such structures by the researchers [1–6] and many works were devoted to this issue [7–14]. Besides the investigations on masonry structures such as destructive, semi-destructive and non-destructive testing; there are also available formulae and tables representing the strength of masonry walls by the strength of masonry components separately. Since masonry is a composite body out of unit and mortar, the researchers state that, the most realistic strength result could be obtained when the combined behavior of masonry unit and masonry mortar is well represented [15]. Even after detecting the effective strength of a masonry structure, a new question *i.e.* suitable method for its strengthening appears.

Nowadays, one of the widely used reinforcing methods for strengthening damaged concrete and masonry structures is the use of Fiber Reinforced Polymers (FRP) in the form of plaster nets [16]. These polymers are applied as embedded meshes within the cement based plasters on the structure's surface, and are commonly available in two different geometries *i.e*. grid texture or a striped texture as illustrated in Figure 1.

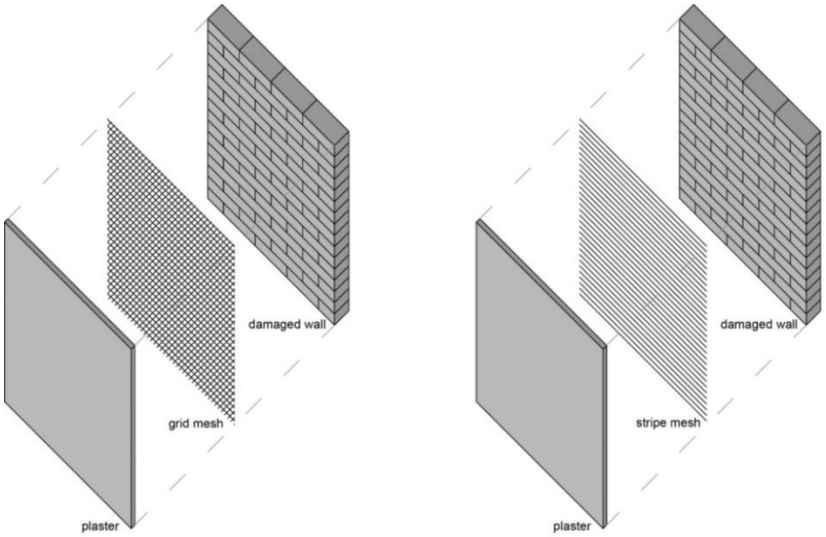

Figure 1: Grid and stripe textured FRP meshes within the plaster

The FRP nets are produced out of different materials such as carbon, glass, basalt and steel fibers in order to achieve the desired strength and compatibility with the deteriorated structures [17, 18]. Although many researchers have already focused on the relation of reinforced concrete structures and FRP based strengthening techniques, this relation is not well studied yet and hence not clear for the masonry structures. The available studies point out that a serious increase could be achieved in the strength of masonry with the help of FRP meshes [19–26]. Although, most of these studies determined the ultimate destructive loads and types of failures under various reinforcement technologies, they did not well define the comparative behavior of different reinforcing materials under one specific condition.

Lastly it was clearly shown that the performance of the strengthening system strongly depends on the accuracy of the installation, the preparation of the substrate surface and the curing condition of the plaster [20].

A significant amount of researches on FRP strengthening is devoted to their use on protecting the structures against seismic impacts [27–32]. The results show that; seismic resistance of masonry structures can be substantially improved with proper use of FRPs. On the other hand, it is a known fact

that, masonry has different behaviors under static and dynamic loads. Although many studies focused on strengthening for dynamic loads, this relation still requires to be studied in terms of static loads.

Lastly, in addition to the seismic studies, FRP strengthening can also propose opportunities in the field of reuse of construction materials. It is a known fact that, many concrete and masonry buildings are either deconstructed or demolished, though their component material still has good quality. Even though the separated material still has good quality; their re-integration as a new component can require alternative techniques in order to achieve the expected unity and strength. From this perspective, the FRP meshes appear as a featured way to sustain the unity between the recovered materials as a new component.

Besides the alternative studied explained above, the main hypothesis of this study was clarified as that; the combined behavior of strengthening intervention and masonry structure in the yielding zone is influenced more by the elastic modulus rates of the FRP and the masonry structure than the strength capacity of the FRP mesh. Therefore, in this paper deformation characteristics of a masonry structure and different types of FRP meshes as well as their combined behavior were analyzed in numerical manners. Hence, the objectives of the study can shortly be noted as follows:

- Evaluation of non-linear behavior of a masonry structure under eccentric loading, that is reinforced by different types of FRP meshes
- Comparison of different stress-strain states of this structure
- Determination of relative deformations of the FRP meshes and the adjacent masonry wall
- Determination of the impacts of FRP mesh addition, to a material reuse project as a case study

2. Methods

A masonry model was used considering its non-linear behavior for the simulation. The model was constructed in Abaqus 6.14 Software, using so-called “Extended” Finite Element Method that takes the initiation possibility of cracks and their growth, into account [33].

The simulation was carried out in a plane problem formulation. The eccentrically loaded masonry wall (under the combined action of compression and bending) was analyzed. The analytical model included a masonry wall element, concrete distribution plate [through which the load was transferred] and a composite reinforcing mesh that is rigidly connected to the masonry as illustrated in Figure 2. Under the proposed loading configuration, the expected deformation is also illustrated in the Figure.

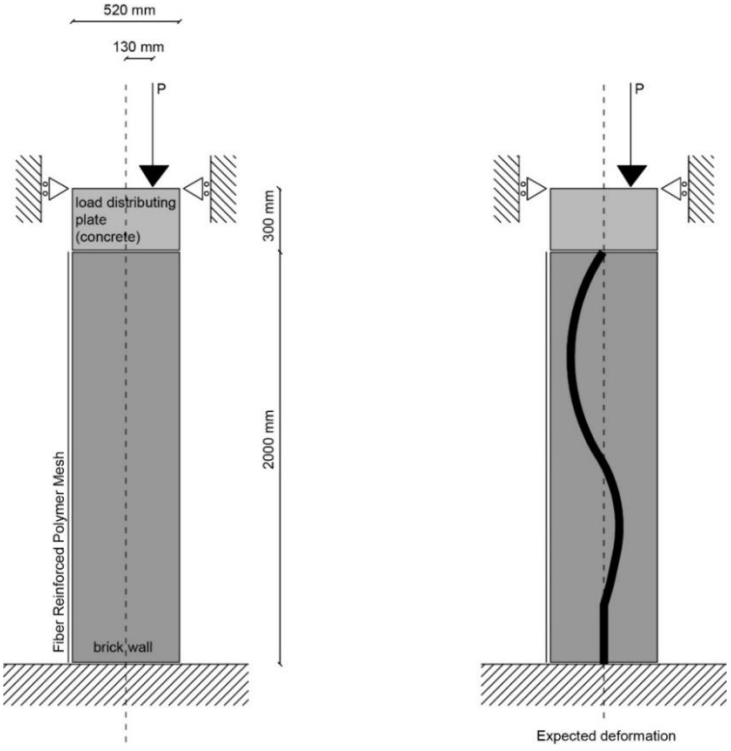

Figure 2. Schema of the masonry wall model used for the simulation

Беспалов В.В., Ючер Д., Салманов И.Д., Курбанов И.Н., Купавых С.В. Деформационная совместимость каменной кладки с композитными материалами // Инженерно-строительный журнал. 2018. № 2(78). С. 136–150.

Seven models based on different FRP reinforcement types were used: Basalt grid (BFRP grid), Aramid stripe (AFRP grid), Natural fiber grid (NFRP grid), Glass fiber grid (GFRP grid), Glass fiber stripe (GFRP stripe), Carbon fiber grid (CFRP grid) and Carbon fiber stripe (CFRP stripe). Additionally, a reference model *i.e.* unreinforced (plain) masonry was obtained for the sake of comparisons. The characteristics of the materials given Table 1 were adopted from the studies of other researchers [6, 34].

Table 1. Mechanical properties of considered materials [Adapted from reference 6, 29]

Material	Modulus of elasticity, E	Poisson coefficient, ν	Tensile strength, σ_t	Compressive strength, σ_c
	GPa	–	MPa	MPa
Basalt (grid)	85	–	400	–
Aramid (stripe)	120	–	320	–
Natural fiber (grid)	25	–	180	–
Glass fiber (grid)	70	–	280	–
Glass fiber (stripe)	105	–	250	–
Carbon fiber (grid)	230	–	350	–
Carbon fiber (stripe)	280	–	350	–
Plain Masonry	25	0.2	0.1	2

Non-linear behavior of the masonry wall under compression was specified by the piecewise approximation based on deformation characteristics of the masonry sample as shown in Figure 3, according to the data obtained from the other studies [14, 35]. When the data from these studies were used for simulation, it is found that a crack is initiated in the masonry element as soon as the tensile stress reaches to 0.1 MPa. Additionally, the stresses in the masonry element were redistributed when the crack appears.

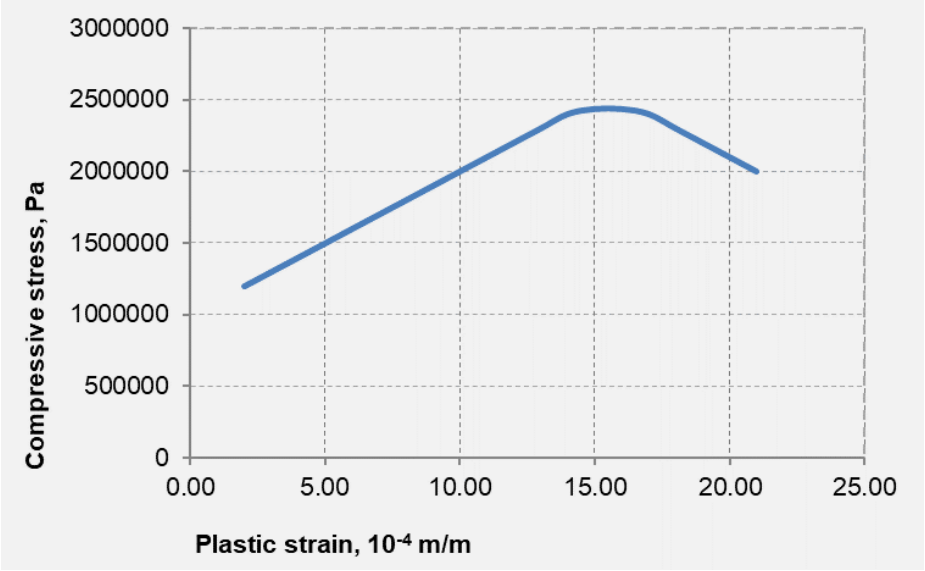

Figure 3. Plasticity diagram of the masonry wall sample

Lastly, a case simulation was completed in order to see how FRP mesh addition can add to a material reuse project. A study completed by a group of researchers offers a recovery project for the debris came out from the demolition of a brick masonry building [36]. In this study, the broken wall pieces (out of solid brick and cement based mortar) were collected from the accumulated debris and they were shaped in order to obtain prismatic blocks for compressive and shear tests as illustrated in Figure 4 and the test results were presented in Table 2.

Figure 4. Accumulated brick debris on the demolition plot, prism preparation for compression and shear test and test set-ups

Table 2. Test results of compression[1] (upper side) and shear blocks[2] (lower side) [31]

Prism	Area [cm^2]	Load [kN]	$F_{mt\ sample}$ [kN/cm^2]	K	$F_{mt\ corrected}$ [MPa]
1	408.59	575	1.41	0.75	10.55
2	401.77	435	1.08		8.12
3	436.77	432.5	0.99		7.43

Mean	8.70	sd	1.34	COV	0.15

Prism	A_1+A_2 [cm^2]	F [kN]	F_{0i} [MPa]
4	484.77	11.66	0.24
5	472.33	5.33	0.11
6	428.33	6.00	0.14

Mean	0.16
sd	0.05
COV	0.33

[1] According to the researchers of the reference study [36], compression test was done according to ASTM C1314: Standard Test Method for Compressive Strength of Masonry Prisms (2014) and K is the correction factor to convert the obtained prism results into standard cube strength. K is dependent on the proportions of the prism, the prisms for this research was 20x20x20 cms and the closest available proportion was 1:1.3 with 0.75 constant value.

[2] Reference study [36] states that, EN 1052-3: Methods of Test for Masonry, Part 3: Determination of Initial Shear Strength (2007) was used as shear test method.

Беспалов В.В., Ючер Д., Салманов И.Д., Курбанов И.Н., Купавых С.В. Деформационная совместимость каменной кладки с композитными материалами // Инженерно-строительный журнал. 2018. № 2(78). С. 136–150.

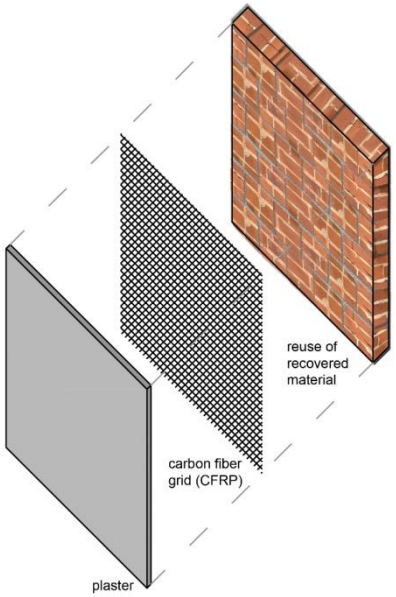

Figure 5. The schema for the material reuse case simulation

As stated in Table 2, the mean compressive strength of these blocks are 8.70 MPa while the mean shear strength for the bed mortar of them is 0.16 MPa. Although both values are quite promising in terms of reusability according to the limit definitions in the sources[3], the integrity of these blocks as a new wall is a question to be answered. One featured answer is the use of FRP meshes as a plaster net for better bonding characteristics as illustrated in Figure 5, obtained according to the system noted in Figure 1. Consequently, the test results obtained from the recovered blocks presented in Table 2 were used for the simulation of a masonry wall with the addition of Carbon fiber grid (CFRP) according to the loading schema given in Figure 2. The outcomes obtained from this simulation are presented in the results section and their comparison with the default values are presented in the discussion section.

3. Results and Discussion

The results obtained from the simulations belong to the mid height of the masonry element on the compressive zone side (the wall surface without the reinforcement) as illustrated in Figure 6. The diagrams in this figure illustrate Strain, ε_{yy}, on X axis versus Stress, σ_{yy}, on Y axis. As seen in this Figure, there are sudden changes in all diagrams that are stress jumps caused by crack initiation and resultant sudden redistribution of stresses. Larger amplitude of jump with an earlier time of the crack is distinctive for FRP with a higher modulus of elasticity as the graphs of glass fiber stripe or carbon fiber grid reinforced masonry walls illustrate in Figure 6. This big-scale stress jump reflects the initiation of the main crack, sharp decrease in the cross section and local strength loss for the masonry element in the compressed zone. When the stress increases again, the jump is completed as a result of the inclusion of adjacent masonry region in plastic state. Moreover, the second jump in the diagrams reflects the occurrence of a new large crack and one more strength loss for the masonry wall. This dual crack formation is not observed in plain masonry wall and its destruction starts with the first main crack as illustrated with a model in Figure 8.

Lastly, the expected depth of cracks are shown with the stress distribution schema in Figure 7. (Embedded within Figure 6). In general, crack formations were local and took almost the same form in each FRP type in the final stage, except aramid and glass fiber stripes. In these two cases, the main crack appeared and passed through 60 % of the section.

[3] The researchers of the reference study [36] concluded that, the compressive strength value obtained from the direct tests on the prisms (shaped wall sections) is higher compared to the allowable strength value indicated in related national standard [37]. This document defines the allowable masonry wall strength according to a formula based on the strengths of brick and mortar. The researchers checked the brick and mortar strengths one by one as well as wall prims for the comparison [36]. Additionally, the researchers stated that, the shear value obtained from the tests is higher compared to the limiting value defined in Eurocode 6, Design of Masonry Structures – Part 1-1: General Rules for Reinforced and Unreinforced Masonry Structures (1996).

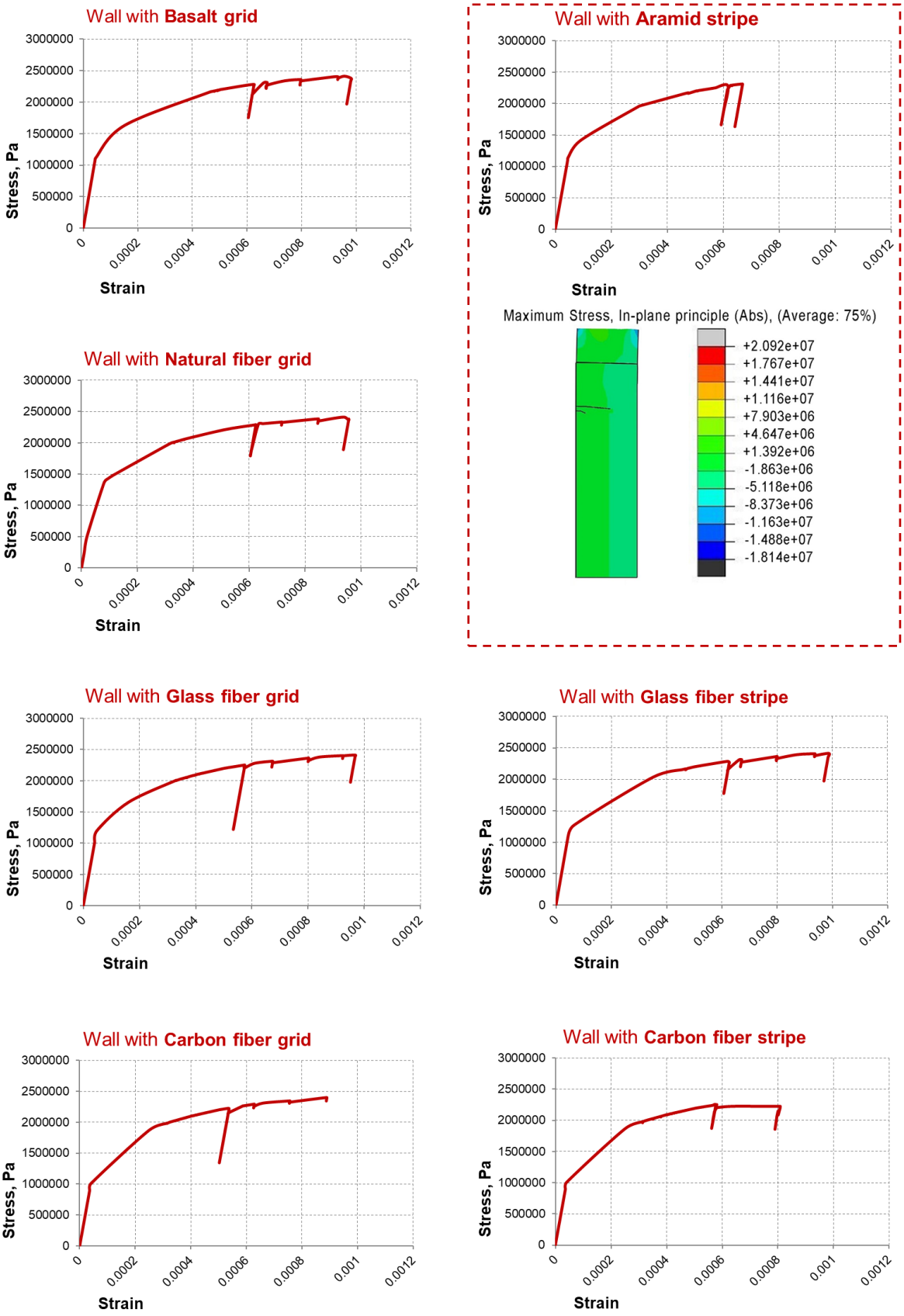

Figure 6. Stress-strain diagrams for compressive zone

Беспалов В.В., Ючер Д., Салманов И.Д., Курбанов И.Н., Купавых С.В. Деформационная совместимость каменной кладки с композитными материалами // Инженерно-строительный журнал. 2018. № 2(78). С. 136–150.

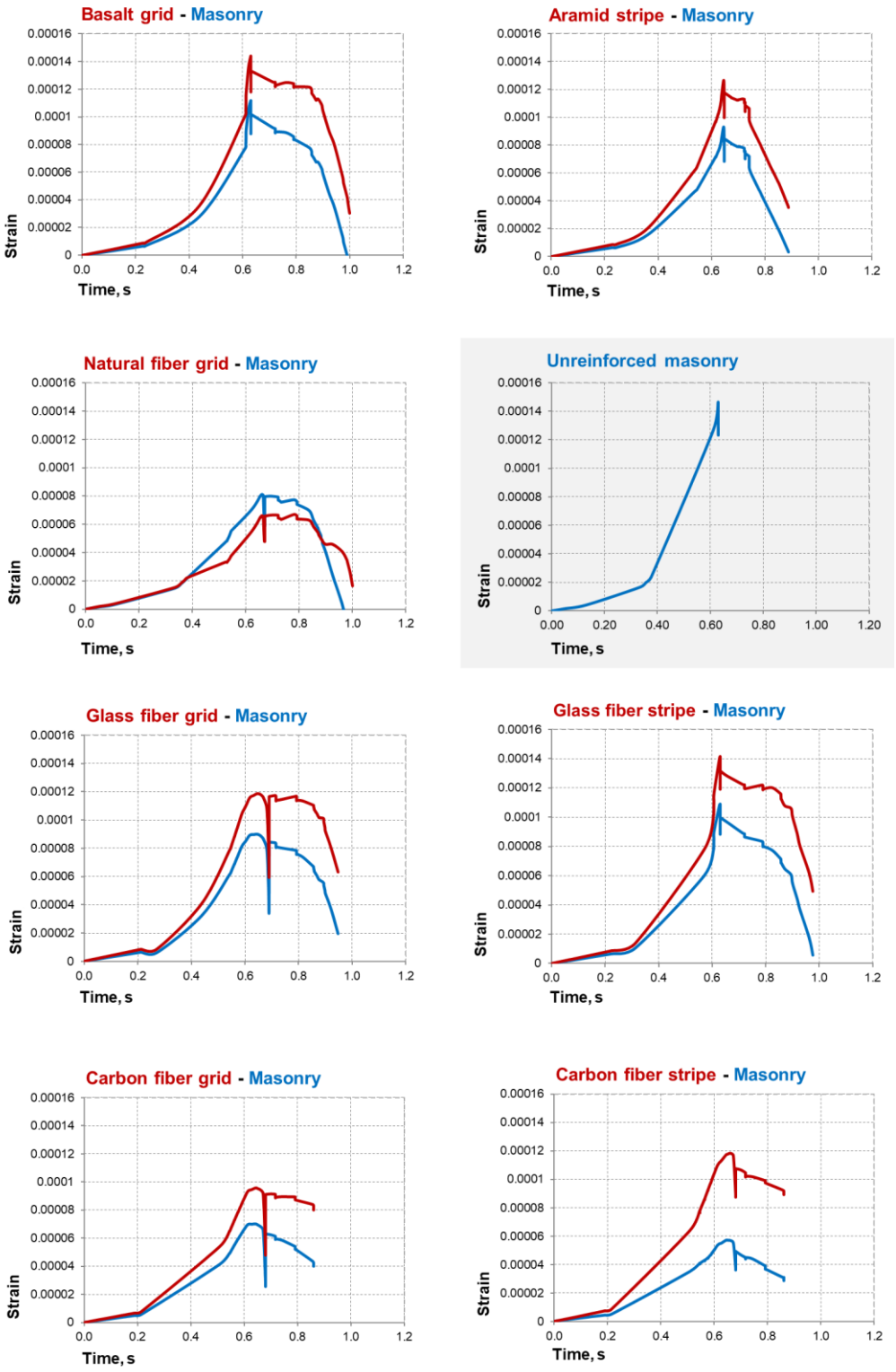

Figure 8[4]. Deformation of the FRP meshes and the adjacent masonry walls, tension zone

Diagrams showing the deformation of FRP meshes and the adjacent masonry walls in tension zone were plotted in Figure 8 to analyze the possible slippage of the mesh and its full separation from the masonry body. These diagrams reflect the deformation levels in FRP and the masonry when the load reaches to maximum.

[4] Diagram for Naural fiber mesh reinforced wall is opposite of the others in terms of capacity comparison of the masonry wall and the reinforcement. This result is expected since this mesh type has quite low modulus of elasticity.

Lastly, the results obtained from the simulation of the case study wall *i.e.* the masonry body out of recovered wall sections is given in Figure 9. The compressive strength value that was obtained from direct test of wall prism *i.e.* 8.7 MPa was used to derive and calculate the modulus of elasticity according to the formula given below[5]:

$$E = f_{mt} * \alpha \\ = 8.7 * 1000 \\ = 8700\ MPa, \quad (1)$$

[37]

where $\alpha = 1000$ is elastic characteristic of masonry with mortar type M10[6]

Lastly the tensile strength of recovered masonry wall was assumed same as the sample wall (0.1 MPa), while the mean shear strength value 0.16 MPa (Table 2) was used as the modeling parameter in Software. The two diagrams plotted in this Figure illustrate the stress-strain diagrams for the unreinforced wall and its strengthened version with carbon fiber grid mesh.

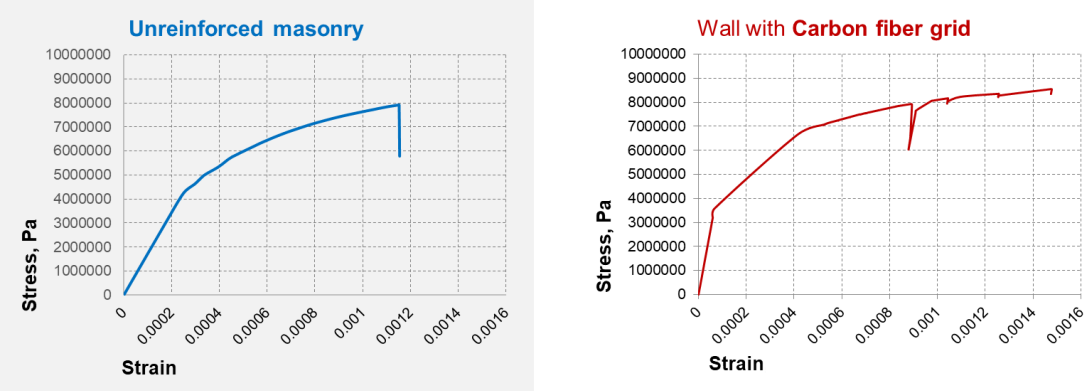

Figure 9. Stress – strain diagram of the recovered masonry wall on the left hand side and its reinforced version with CFRP grid mesh on right hand side

These two diagrams in Figure 9 illustrate that; the reinforced wall has slightly larger stress capacity *i.e.* the maximum stress for unreinforced version is about 8.0 MPa while the reinforced one can reach up to about 8.5 MPa. Additionally, the strain capacity of reinforced one reaches to 0.0015 mm while the unreinforced one is about 0.0011 mm. Moreover, the unreinforced masonry is rapidly destroyed by the crack growth in the tension zone that results in critical cross sectional reduction, which is visible with the sharp fall in the diagram, while the reinforced wall can keep the bearing capacity even after the first fall *i.e.* first main crack in the diagram as seen in Figure 9. In the reinforced case, the CFRP mesh prevents the growth of the first main crack at a certain stage that appears as a jump in the stress diagram for the reinforced wall. Since the main crack is restrained, the bearing capacity of the masonry wall slightly increases until the appearance of new cracks. These new cracks are also neutralized by the reinforcement until the fourth main crack as illustrated in Figure 10 and their reflectance as small stress jumps in Figure 9.

Lastly, when the comparative crack formations are analyzed for these two wall options, it is clear that only one single region occurs for the plain wall while this region is reduced and divided into two, for the reinforced alternative as seen in Figure 10.

In plain masonry wall case, there is no source for significant shear stress as seen in Figure 11. Additionally, the shear failure occurs in the reinforced surface of the masonry wall when the tangential stresses reaches to shear strength limit, since FRP cannot provide its full strength capacity. The FRP could provide the best performance when its modulus of elasticity is close to masonry wall, in other words the two components are compatible in terms of deformation properties.

One final aspect to be clarified is the behaviors of recovered masonry wall and the CFRP reinforcing grid mesh. Their diagrams in terms of time and deformation are given in Figure 12 below. These diagrams are presented in order to have an opinion on their compatibility as well as the

[5] National Standard [SNIP II-22-81], (2012).

[6] The mean compressive strength of mortar obtained from direct tests is convered into 14.13 MPa cube strength [36] and it falls into M10 type.

comparison to the sample wall and different reinforcement alternatives on it, as explained in the previous sections of this study.

Unreinforced masonry time-strain diagram here and time-strain diagram for masonry and carbon fiber grid mesh together (as the diagrams in Figure 8), the tension zone.

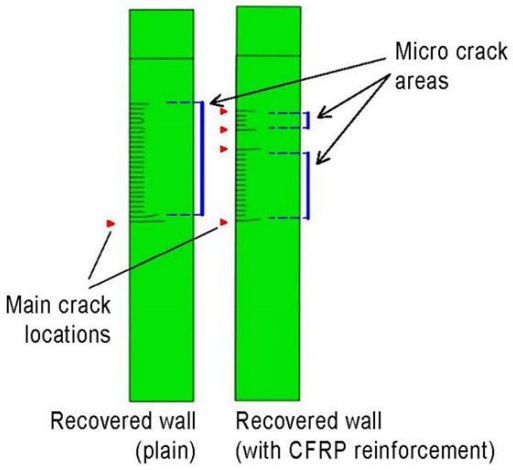

Figure 10. Simulation of cracks for recovered wall

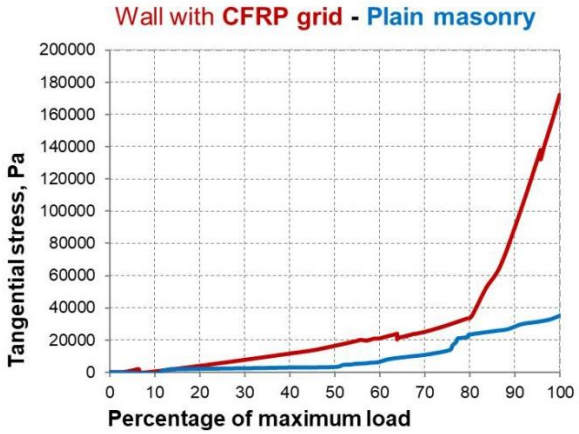

Figure 11. Tangential stress diagram for recovered wall (tension side)

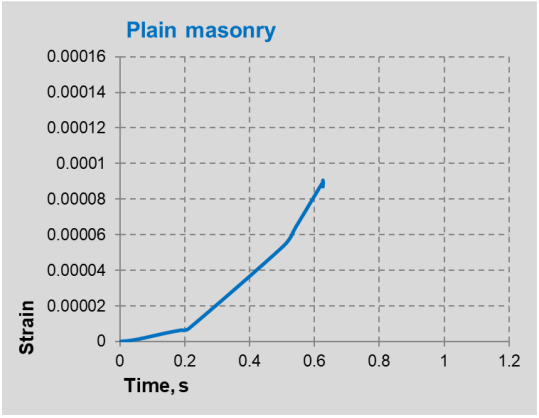

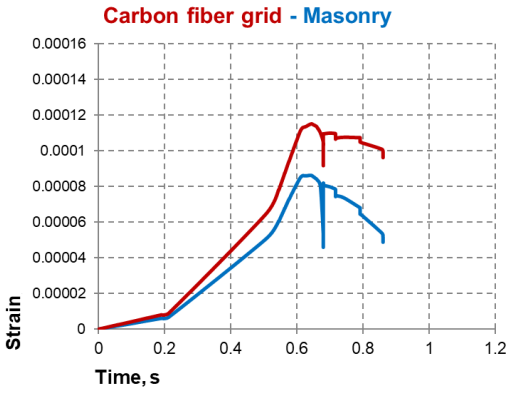

Figure 12. Deformation of recovered masonry wall on the left hand side, and Deformation of the CFPR mesh and the adjacent recovered masonry wall on the right hand side, tension zone

Following the analysis on seven different FRP meshes and their behaviors on a masonry wall sample as well as a recovery case study with and without CFRP reinforcing, all data obtained from the simulations are discussed in the following section.

All the separate stress-strain diagrams obtained from the simulation of seven different FRP meshes on the sample masonry wall are gathered in Figure 13, for the sake of comparison. The curves are of similar nature, but the difference in the appearance of spikes and the formation of the fracture cracks are clearly distinguishable in this Figure. Comparatively the earliest formation of a crack was observed in a model with carbon fiber grid reinforcement (stripe version is also one of the earliest cracks), while the latest first jump *i.e.* latest crack appeared in the basalt fiber grid reinforcing model. The first jumps of the NFRP grid and AFRP stripe reinforced masonry walls are located almost in the same point. Lastly, the largest amplitude of the jump occurred in the masonry model with GFRP grid reinforcement.

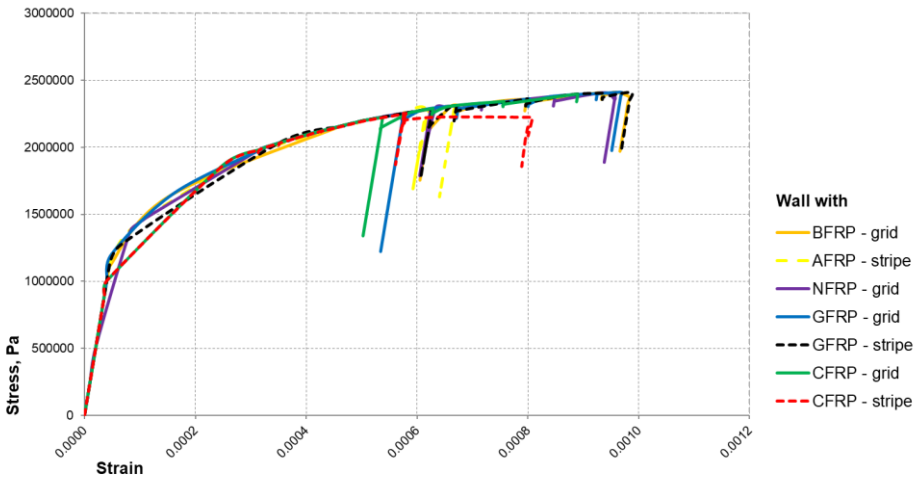

Figure 13. Stress-strain diagram of reinforced masonry alternatives in compression zone

Aramid and glass fiber stripe reinforced masonry walls experienced large cracks that are deeper than 60 % of the wall section but there is no explicit reflection of this on their stress-strain states as shown in Figure 13. This could be interpreted as that, the cracks reached to this significant depth only after the second stress jump was passed, namely; the samples reached their limits of bearing capacity on the second sharp fall. In case of aramid and glass fiber stripe, this second sharp fall resulted in fast growth of the first main crack, instead of initiation of new big crack as appeared in the other cases.

Diagrams in Figure 8 show that, the difference in deformation of the reinforcement mesh and the adjacent masonry wall reaches to significant values in some cases (as seen in pre-crack part of strain diagrams and especially in case of CFRP stripe, where strain difference grows up long before the initiation of the first main crack). As an example, the deformation of CFRP stripe mesh is twice as large as the deformation of the adjacent masonry wall, which can cause the slippage of the reinforcement from the surface. Although it is not possible to determine the relative strain difference resulting in slippage, with the help of a numerical model, where the experimental data from the real samples are compulsory; it is possible to detect the relative deformation compatibilities from the strain diagrams. Thus, the simplest expression of the deformation compatibility is the sum of the difference between relative strains of reinforcement and masonry wall; as noted in Formulae 2 and 3.

$$\alpha = \int_0^1 \Delta\varepsilon dt, \tag{2}$$

where α – Deformation compatibility;

$\Delta\varepsilon = \left|\varepsilon^{FRP} - \varepsilon^{M}\right|$ – Strain difference of reinforcement and masonry body.

Using the relative strain values can be a logical way to compare the deformation compatibility of the masonry body and the reinforcing mesh, as noted in Formula 3. The closer this value is to 1.0, the higher the relative deformation compatibility.

$$\alpha_{rel} = 1 - \left(\sum_i \left(\left|\varepsilon_i^{FRP} - \varepsilon_i^{M}\right| \times t_i\right)\right) \times 10^4 \tag{3}$$

where α_{rel} – relative deformation compatibility;

i – Number of calculation iterations, where the deformation of the masonry wall and the reinforcing meshes are calculated in each step;

t_i – Duration of each iteration

Lastly, relative deformation compatibility values of seven different FRP meshes, analyzed in this study were calculated according to the suggested formula above, and the results are given in Table 3.

Table 3. Deformation compatibility of different FRP meshes

Reinforcement Type	Maximum strain difference, $\Delta\varepsilon_{max}$	Value of relative deformation compatibility, α_{rel}
BFRP (grid)	$4.63 \cdot 10^{-5}$	0.786
AFRP (stripe)	$3.51 \cdot 10^{-5}$	0.855
NFRP (grid)	$4.72 \cdot 10^{-5}$	0.898
FGRP (grid)	$4.54 \cdot 10^{-5}$	0.822
FGRP (stripe)	$4.50 \cdot 10^{-5}$	0.794
CFRP (grid)	$4.06 \cdot 10^{-5}$	0.86
CFRP (stripe)	$6.17 \cdot 10^{-5}$	0.715

As noted in Table 3, the maximum strain difference is the lowest for AFRP reinforced model whereas it is the highest for CFRP-stripe reinforced model. Additionally, relative deformation compatibility value is maximum for NFRP-stripe reinforced model, while it is minimum for CFRP reinforced model. These values can be interpreted as that, regarding the low strain difference value and comparatively high relative deformation compatibility value; AFRP features as a favorable application for strengthening the modelled sample masonry wall, among the other alternatives. On the other hand, since both values in question are the maximum ones for CFRP stripe reinforced model, this wall – reinforcement combination appear as the least suitable one. Moreover, this model also demonstrated the earliest fracture crack in stress-strain diagram, in Figure 8, which confirms the incompatibility of its components.

Table 3 indicates a large difference between the calculated values both for maximum strain values and relative deformation compatibility for reinforcing options. This deviation is a direct result of the distinct deformation diagrams of failures for reinforcing options; as already noted in Figure 8.

Lastly, the maximum strain difference and relative deformation compatibility values were calculated for the recovered masonry wall and CFRP grid reinforcement combination; according to the Formulae 2 and 3 as noted in Table 4.

Table 4. Deformation compatibility for recovered wall and carbon fiber based reinforcement combination

Reinforcement Type	Maximum strain difference, $\Delta\varepsilon_{max}$	Value of relative deformation compatibility, α_{rel}
CFRP – grid	$5.14 \cdot 10^{-5}$	0.842

Although only one type of reinforcement was modelled for the recovered masonry wall, these two values were still obtained in order to have a broad opinion on their comparison with the sample wall models noted in Table 3. The maximum strain difference is $5.14 \cdot 10^{-5}$ where the compatibility deformation value is 0.842. When these values are compared with the values for the sample wall in Table 3, two options appear. The maximum strain value obtained from CFRP grid on the recovered wall is between the CFRP strip and the CFRP grid on the sample wall. Although the relative deformation compatibility of CFRP grid on the recovered wall is closest to the AFRP strip on the sample wall, the value from CFRP grid on the sample wall is also very close. Consequently, regarding these two parameters together, the behavior and crack formation expectation for the CRRP grid on recovered wall would be most similar to the CFRP grid reinforcement on the sample wall.

After obtaining strain difference and relative deformation compatibility values for the sample and the recovered masonry walls, the comments and summaries are presented in the following section.

4. Conclusions

The featured outcomes obtained by this study were presented and explained one by one in the following text.

1. Stress-strain state and deformation compatibility of different fiber reinforced polymer (FRP) reinforcement types for masonry walls under eccentric load were obtained.

2. Stress jump reflecting the initiation of a main crack was presented as a possible way for determining the limit bearing capacity of FRP reinforced masonry walls.

3. Different behaviors of representative masonry wall with and without FRP strengthening in the post-peak stage was determined. It was obtained that, the emergence of the main crack protects the wall from further damage and allows the strength contribution of the neighboring sections of the wall, when the reinforcement is present. On the other hand, the main crack results in the rapid destruction of the structure, if there is no reinforcement.

4. Although this outcome requires further inquiry with real experiments, the simulation model illustrated that the main cracks continue more than 60% of the wall cross section; as obtained for AFRP and GFRP stripe reinforcement cases.

5. It is shown that, the deformation diagrams of FRP meshes and the masonry wall can be used as a tool for determining their relative deformation compatibility. Additionally, this compatibility was pointed as the key element during the suitable reinforcement type selection according to the deteriorated wall in question.

6. Although the FRP reinforcing resulted in a slight strength capacity increase in the reclaimed wall alternative (case study), its main impact appeared as increasing the ductility of the wall. The wall model without reinforcement showed a brittle, sudden failure while the reinforced case could keep its unity for a while even after the failure. This is a life-saving property for the structural elements, when the case is sustaining enough time for inhabitants to escape before the failure.

7. The reinforcing mesh on the recovered wall case could have provided better shear strength behavior (since it has larger capacity) if its properties were more similar to the wall's deformation characteristics.

8. The values of maximum strain difference and the relative deformation compatibility for the CFRP reinforced, recovered wall case was closest to the CFRP stripe strengthened sample masonry wall. These approximate values are pointed as expectable behavior similarities for these two cases.

In brief, besides the 8 items noted above, the simulation software used for this study (Abaqus) showed its usefulness in terms of deformation compatibility calculations. On the other hand, the verification and refinement of the simulation results as well as combined behavior detection of masonry and reinforcement mesh (especially under compression and bending) require full scale experiments.

References

1. Bespalov V.V., Zimin S.S. The strength of masonry vaulted structures. *Construction of Unique Buildings and Structures.* 2016. No. 11(50). Pp. 37–51. (rus)
2. Zimin S.S., Kokotkova O.D., Bespalov V.V. Vault structures of historical buildings. *Construction of Unique Buildings and Structures.* 2015. No. 2(29). Pp. 57–72. (rus)
3. Zimin S.S., Bespalov V.V., Skripchenko I.V. Spandrels influence on the stress state of masonry vaults. *Obsledovanie zdanij i sooruzhenij: problemy i puti ih resheniya: Materialy VII mezhdunarodnoj nauchno-prakticheskoj konferencii.* Izd-vo SPbGPU, 2017. Pp. 133–144. (rus)
4. Skripchenko I.V., Bespalov V.V., Lukichev S.Y., Zimin S.S. Unconventional cases of the stone vaults. *Construction of Unique Buildings and Structures.* 2017. No. 2(53). Pp. 87–95.
5. Bespalov V., Orlovich R., Zimin S. Stress-Strain State of Brick Masonry Vault with an Aperture. *MATEC Web of Conferences.* 2016. No. 53. 01009.
6. Sousa R., Guedes J., Sousa H. Characterization of the uniaxial compression behavior of unreinforced masonry–Sensitivity analysis based on a numerical and experimental approach. *Archives of Civil and Mechanical Engineering.* 2015. No. 15. Pp. 532–547.
7. Ulybin A.V., Startsev S.A., Zubkov S.V. Humidity control in the inspection of masonry structures. *Magazine of Civil Engineering.* 2013. No. 7(42). Pp. 32–39. (rus)
8. Silva B., Pappas A., Valluzzi, M.R., Porto F., Modena C. Calibration of a numerical material behaviour model for the simulation of multi-leaf stone masonry walls. *Structural Analysis of Historical Constructions.* 2012. Pp. 575–583.
9. Bisoffi-Sauve M. *Etude des ouvrages maçonnés en pierre*

Литература

1. Беспалов В.В., Зимин С.С. Прочность каменной кладки сводчатых конструкций // Строительство уникальных зданий и сооружений. 2016. № 11(50). С. 37–51.
2. Зимин С.С., Кокоткова О.Д., Беспалов В.В. Сводчатые конструкции исторических зданий // Строительство уникальных зданий и сооружений. 2015. № 2(29). С. 57–72.
3. Зимин С.С., Беспаолв В.В., Скрипченко И.В. Влияние распалубок на напряженное состояние каменных сводов // Материалы VII международной научно-практической конференции (Обследование зданий и сооружений: проблемы и пути их решения). СПб.: Изд-во СПбПУ, 2017. С. 133–144.
4. Скрипченко И.В., Беспалов В.В., Лукичев С.Ю., Зимин С.С. Нетипичные случаи каменных сводов // Строительство уникальных зданий и сооружений. 2017. № 2(53). С. 87-95.
5. Bespalov V., Orlovich R., Zimin S. Stress-Strain State of Brick Masonry Vault with an Aperture // MATEC Web of Conferences. 2016. No. 53. 01009.
6. Sousa R., Guedes J., Sousa H. Characterization of the uniaxial compression behavior of unreinforced masonry–Sensitivity analysis based on a numerical and experimental approach // Archives of Civil and Mechanical Engineering. 2015. №15. Pp. 532–547.
7. Улыбин А.В., Старцев С.А., Зубков С.В. Контроль влажности при обследовании каменных конструкций // Инженерно-строительный журнал. 2013. № 7(42). С. 32–39.
8. Silva B., Pappas A., Valluzzi M.R., Porto F., Modena C. Calibration of a numerical material behaviour model for the simulation of multi-leaf stone masonry walls // Structural

Беспалов В.В., Ючер Д., Салманов И.Д., Курбанов И.Н., Купавых С.В. Деформационная совместимость каменной кладки с композитными материалами // Инженерно-строительный журнал. 2018. № 2(78). С. 136–150.

par la méthode des éléments discrets: caractérisation et modélisation du comportement cohésif des joints. Mécanique des structures. Ph.D. Thesis. Universite de Bordeaux. 2016. 191 p.
10. Bisoffi-Sauve M. Caractérisation et modélisation des joints de mortier dans les structures maçonnées en pierre. *34èmes Rencontres de l'AUGC.* Université de Liège, Belgique. 2016. Pp. 1–8.
11. Villemus B. Etude des murs de soutenement en maconnerie de pierres seches. Ph.D. Thesis. *Ecole L'institut National des Sciences Appliquees de Lyon.* 2004. 254 p.
12. Bagneris M., Dubois F., Martin A. Numerical analysis of historical masonry structures for stone degradation diagnosis: An application to the Roman Amphitheater of Nîmes. *Digital Heritage.* 2013. Pp. 521–528.
13. Tabbakhha M. *Multiscale methodology for vulnerability assessment of masonry structures.* Ph.D. Thesis. Ecole Centrale Paris. 2013. 241 p.
14. Derkach V.N. *Kamennoye zapolneniye karkasnykh zdaniy: prochnost, zhestkost i silovoye vzaimodeystviye s karkasom* [Masonry filling of frame buildings: strength, stiffness and force interaction with the frame]. D.Sc Thesis. Brest, 2016. 260 p. (rus)
15. Zubkov S.V., Ulybin A.V. and Fedotov S.D., Assessment of the mechanical properties of brick masonry by a flat-jack method. *Magazine of Civil Engineering.* 2015. No. 8. Pp. 20-29.
16. Parghi A., Alam S. A review on the application of sprayed-FRP composites for strengthening of concrete and masonry structures in the construction sector. *Composite Structures.* 2018. No. 187. Pp. 518–534.
17. Shaw I., Andrawes B. Repair of damaged end regions of PC beams using externally bonded FRP shear reinforcement. *Construction and Building Materials.* 2017. No. 148. Pp. 184–194.
18. Gattulli V., Lampis G., Marcari G., Paolone A. Simulations of FRP reinforcement in masonry panels and application to a historic façade. *Engineering Structures.* 2014. No. 75. Pp. 604–618.
19. Valluzzi M.R., Binda L., Modena C. Mechanical behaviour of historic masonry structures strengthened by bed joints structural repointing. *Construction and Building Materials.* 2005. No. 19. Pp. 63–73.
20. Bernat-Maso E., Escrig C., Aranha C.A., Gil L. Experimental assessment of Textile Reinforced Sprayed Mortar strengthening system for brickwork wallettes. *Construction and Building Materials*. 2014. No. 50. Pp. 226–236.
21. Shaheen E., Shrive N.G. Strengthening of masonry columns with sprayed glass fibre reinforced polymer (SGFRP). *10th Canadian Masonry Symposium.* Banff, Alberta. 2005. Pp. 1–10.
22. McGinley W.M., Corzo A.M., Gergely J., Foster P.B., Young D.T. A design methodology for FRP systems for masonry structures. *10th Canadian Masonry Symposium.* Banff, Alberta. 2005. Pp. 34–44.
23. Zanaz A. *Approche probabiliste d'aide au diagnostic des voûtes en maçonnerie.* Ph.D. Thesis. Université de Limoges. 2016. 208 p.
24. Este A., Toson B., Saliba J., El Yagoubi J., Mindeguia J.-C., Martin E., Morel S. A new approach to simulate interface damage in brittle matrix composites. *Procedia Structural Integrity.* 2016. No. 2. Pp. 2456–2462.
25. Bernat-Maso E., Escrig C., Aranha C.A. Construction Experimental assessment of Textile Reinforced Sprayed Mortar strengthening system for brickwork wallettes. *Building Materials.* 2013. No. 50. Pp. 226–236.
26. De Santis S., De Felice G. Bond behaviour of steel reinforced grout strengthening systems applied to the extrados of masonry vaults. *Structural Analysis of Historical Constructions.* 2016. Pp. 344–350.
27. Garmendia L., San-Mateos R., García D., Gandini A., San-José J.T., Marcos I. Retrofitting of masonry vaults with composite materials. *Structural Analysis of Historical* Analysis of Historical Constructions. 2012. Pp. 575–583.
9. Bisoffi-Sauve M. Etude des ouvrages maçonnés en pierre par la méthode des éléments discrets: caractérisation et modélisation du comportement cohésif des joints. Mécanique des structures. Ph.D. Thesis. Universite de Bordeaux. 2016. 191 p.
10. Bisoffi-Sauve M. Caractérisation et modélisation des joints de mortier dans les structures maçonnées en pierre. 34èmes Rencontres de l'AUGC. Université de Liège, Belgique. 2016. Pp. 1-8.
11. Villemus B. Etude des murs de soutenement en maconnerie de pierres seches. Ph.D. Thesis. Ecole L'institut National des Sciences Appliquees de Lyon. 2004. 254 p.
12. Bagneris M., Dubois F., Martin A. Numerical analysis of historical masonry structures for stone degradation diagnosis: An application to the Roman Amphitheater of Nîmes // Digital Heritage. 2013. Pp. 521–528.
13. Tabbakhha M. Multiscale methodology for vulnerability assessment of masonry structures. Ph.D. Thesis. Ecole Centrale Paris. 2013. 241 p.
14. Деркач В.Н. Каменное заполнение каркасных зданий: прочность, жесткость и силовое взаимодействие с каркасом. Дисс. д.т.н. Брест, 2016. 260 с.
15. Зубков С.В., Улыбин А.В., Федотов С.Д. Исследование механических свойств кирпичной кладки методом плоских домкратов // Инженерно-строительный журнал. 2015. № 8(60). С. 20–29.
16. Parghi A., Alam S. A review on the application of sprayed-FRP composites for strengthening of concrete and masonry structures in the construction sector // Composite Structures. 2018. № 187. Pp. 518–534.
17. Shaw I., Andrawes B. Repair of damaged end regions of PC beams using externally bonded FRP shear reinforcement // Construction and Building Materials. 2017. № 148. Pp. 184–194.
18. Gattulli V., Lampis G., Marcari G., Paolone A. Simulations of FRP reinforcement in masonry panels and application to a historic façade // Engineering Structures. 2014. № 75. Pp. 604–618.
19. Valluzzi M.R., Binda L., Modena C. Mechanical behaviour of historic masonry structures strengthened by bed joints structural repointing // Construction and Building Materials. 2005. № 19. Pp. 63–73.
20. Bernat-Maso E., Escrig C., Aranha C. A., Gil L. Experimental assessment of Textile Reinforced Sprayed Mortar strengthening system for brickwork wallettes // Construction and Building Materials. 2014. № 50. Pp. 226–236.
21. Shaheen E., Shrive N.G. Strengthening of masonry columns with sprayed glass fibre reinforced polymer (SGFRP) // 10th Canadian Masonry Symposium, Banff, Alberta. 2005. Pp. 1–10.
22. McGinley W.M., Corzo A.M., Gergely J., Foster P.B., Young D.T. A design methodology for FRP systems for masonry structures // 10th Canadian Masonry Symposium, Banff, Alberta. 2005. Pp. 34–44.
23. Zanaz A. Approche probabiliste d'aide au diagnostic des voûtes en maçonnerie. Ph.D. Thesis. Université de Limoges. 2016. 208 p.
24. Este A., Toson B., Saliba J., El Yagoubi J., Mindeguia J.-C., Martin E., Morel S. A New Approach to Simulate Interface Damage in Brittle Matrix Composites // Procedia Structural Integrity. 2016. № 2. Pp. 2456–2462.
25. Bernat-Maso E., Escrig C., Aranha C.A. Construction Experimental assessment of Textile Reinforced Sprayed Mortar strengthening system for brickwork wallettes // Building Materials. 2013. № 50. Pp. 226–236.
26. De Santis S., De Felice G. Bond behaviour of steel reinforced grout strengthening systems applied to the extrados of masonry vaults // Structural Analysis of Historical Constructions. 2016. Pp. 344–350.
27. Garmendia L., San-Mateos R., García D., Gandini A., San-José J.T., Marcos I. Retrofitting of masonry vaults with

Constructions. 2016. Pp. 351–356.
28. Wang X., Ghiassi B., Oliveira D.V. Numerical analysis of the in-plane behaviour of TRM-strengthened masonry walls. *Structural Analysis of Historical Constructions.* 2016. Pp. 365–371.
29. Hojdys L., Krajewski P. Glass fiber grids embedded in a cement-based matrix as strengthening of masonry structures. *Structural Analysis of Historical Constructions*. 2016. Pp. 372–376.
30. Serhal J. *Etude de la vulnérabilité des bâtiments en maçonnerie soumis à des mouvements de terrains et élaboration de critères d'évolution de leur rigidité.* Ph.D. Thesis. Universite de Lorraine. 2016. 188 p.
31. Taforel P., Dubois F., Martin A., Pagano S. Développement de formulations dynamiques adaptées à la modélisation par éléments discrets de structures maçonnées sous chargements sismiques. *10e colloque national en calcul des structures.* 2011. Pp. 1–12.
32. Kabantsev O.V. *Nauchnyye osnovy strukturnoy teorii kamennoy kladki dlya otsenki predelnykh sostoyaniy kamennykh konstruktsiy seysmostoykikh zdaniy* [Scientific basis for the structure theory of masonry for the assessment of limit states of masonry structures for earthquake-resistant buildings]. D.Sc Thesis. Moscow, 2016. 358 p. (rus)
33. Martin A., Esnault J.-B., Massin P. About the use of standard integration schemes for X-FEM in solid mechanics plasticity. *Computer Methods in Applied Mechanics and Engineering.* 2014. Pp. 283–293.
34. *Geometrical and Mechanical properties of the hemp FRP composite.* [Electronic resource]. System requirements: AdobeAcrobatReader. URL: http://www.fidiaglobalservice.com/eng/materiali_schede/FIDHEMP20UNIDIR2024020HS40.pdf (accessed: 19.10.2017).
35. Pelà L. *Continuum damage model for nonlinear analysis of masonry structures.* Ph.D. Thesis. Universitat Politècnica de Catalunya. 2009. 299 p.
36. Ucer D., Ulybin A., Zubkov S., Elias-Ozkan S.T. Analysis on the mechanical properties of historical brick masonry after machinery demolition. *Construction and Building Materials.* 2018. No. 161. Pp. 186–195.
37. *SNIP [II-22-81],* Building Regulations for Stone and Reinforced Masonry Structures, Central Institute of Standard Design [CNIISK Institute], Moscow, [1987], 2012.

composite materials // Structural Analysis of Historical Constructions. 2016. Pp. 351–356.
28. Wang X., Ghiassi B., Oliveira D.V. Numerical analysis of the in-plane behaviour of TRM-strengthened masonry walls // Structural Analysis of Historical Constructions. 2016. Pp. 365–371.
29. Hojdys L., Krajewski P. Glass fiber grids embedded in a cement-based matrix as strengthening of masonry structures // Structural Analysis of Historical Constructions. 2016. Pp. 372–376.
30. Serhal J. Etude de la vulnérabilité des bâtiments en maçonnerie soumis à des mouvements de terrains et élaboration de critères d'évolution de leur rigidité. Ph.D. Thesis. Universite de Lorraine. 2016. 188 p.
31. Taforel P., Dubois F., Martin A., Pagano S. Développement de formulations dynamiques adaptées à la modélisation par éléments discrets de structures maçonnées sous chargements sismiques // 10e colloque national en calcul des structures. 2011. Pp. 1–12.
32. Кабанцев О.В. Научные основы структурной теории каменной кладки для оценки предельных состояний каменных конструкций сейсмостойких зданий. Дис. д.т.н. Москва, 2016. 358 с.
33. Martin A., Esnault J.-B., Massin P. About the use of standard integration schemes for X-FEM in solid mechanics plasticity // Computer Methods in Applied Mechanics and Engineering. 2014. Pp. 283–293.
34. Geometrical and Mechanical properties of the hemp FRP composite. [Электронный ресурс]. Сист.требования: AdobeAcrobatReader. URL: http://www.fidiaglobalservice.com/eng/materiali_schede/FIDHEMP20UNIDIR2024020HS40.pdf (дата обращения: 19.10.2017).
35. Pelà L. Continuum damage model for nonlinear analysis of masonry structures. Ph.D. Thesis. Universitat Politècnica de Catalunya. 2009. 299 p.
36. Ucer D., Ulybin A., Zubkov S., Elias-Ozkan S.T. Analysis on the mechanical properties of historical brick masonry after machinery demolition // Construction and Building Materials. 2018. No. 161. Pp. 186-195.
37. СП 15.13330.2012 «Актуализированная редакция СНиП II-22–81* Каменные и армокаменные конструкции».

Vladimir Bespalov,
+7(981)785-08-99; chanchullero@yandex.ru

Deniz Ucer,
+7(981)956-03-45; deucer@metu.edu.tr

Ildus Salmanov,
+7(911)843-34-26; ildussalmanov@gmail.com

Israfil Kurbanov,
+7(962)715-11-17; Israfil-kurbanov@mail.ru

Svetlana Kupavykh,
+7(812)328-86-74;
Siniavina_SV@pers.spmi.ru

Владимир Владимирович Беспалов,
+7(981)785-08-99;
эл. почта: chanchullero@yandex.ru

Дениз Ючер,
+7(981)956-03-45; эл.почта: deucer@metu.edu.tr

Ильдус Динисламович Сальманов,
+7(911)843-34-26;
эл. почта: ildussalmanov@gmail.com

Исрафил Низамович Курбанов,
+7(962)715-11-17;
эл. почта: Israfil-kurbanov@mail.ru

Купавых Светлана Викторовна
+7(812)328-86-74;
эл. почта: Siniavina_SV@pers.spmi.ru

Беспалов В.В., Ючер Д., Салманов И.Д., Курбанов И.Н., Купавых С.В. Деформационная совместимость каменной кладки с композитными материалами // Инженерно-строительный журнал. 2018. № 2(78). С. 136–150.